A general approach to study molecular fragmentation and energy redistribution after an ionizing event

Ewa Erdmann, Néstor F Aguirre, Suvasthika Indrajith, Jacopo Chiarinelli, Alicja Domaracka, Patrick Rousseau, Bernd A Huber, Paola Bolognesi, Robert Richter, Lorenzo Avaldi, et al.

Cite this: DOI: 00.0000/xxxxxxxxxx

A General Approach to Study Molecular Fragmentation and Energy Redistribution After an Ionizing Event†

Ewa Erdmann,[a,b] Néstor F. Aguirre,[b,c] Suvasthika Indrajith,[d] Jacopo Chiarinelli,[e,f] Alicja Domaracka,[d] Patrick Rousseau,[d] Bernd A. Huber,[d] Paola Bolognesi,[e] Robert Richter,[g] Lorenzo Avaldi,[e] Sergio Díaz-Tendero ,[b,h,i] Manuel Alcamí,[b,h,j] and Marta Łabuda*[a]

Received Date
Accepted Date

DOI: 00.0000/xxxxxxxxxx

We propose to combine quantum chemical calculations, statistical mechanical methods, and photoionization and particle collision experiments to unravel the redistribution of internal energy of the furan cation and its dissociation pathways. This approach successfully reproduces the relative intensity of the different fragments as a function of the internal energy of the system in photoelectron-photoion coincidence experiments and the different mass spectra obtained when ions ranging from Ar^+ to Xe^{25+} or electrons are used in collision experiments. It provides deep insights into the redistribution of the internal energy in the ionized molecule and its influence on the dissociation pathways and resulting charged fragments. The present pilot study demonstrates the efficiency of a statistical exchange of excitation energy among various degrees of freedom of the molecule and proves that the proposed approach is mature to be extended to more complex systems.

1 Introduction

The energy transfer in molecular collisions with photons, electrons and ions and its redistribution among the internal degrees of freedom are key features to understand the radiation-matter interaction, relevant for various disciplines, such as astrophysics, atmospheric science and radiation damage in biological tissues. In the last two decades, considerable progress has been made in the development and application of theoretical and experimental approaches to investigate both the energy transfer and the related electronic and nuclear dynamics. However, as the size of the systems and excitation energy increase, the large number of accessible degrees of freedom and competing fragmentation channels make this issue more and more challenging. The distribution of the energy transferred in ion collision experiments has been previously obtained by a measurement in coincidence of the projectile charge state and energy loss, of the fragmentation mass spectrum and of the electron emission [1,2] or via a combination of photon and ion experiments [3]. Theoretical determinations of the deposited energy were obtained by the calculation of the nuclear and electronic stopping powers [4] or by the evaluation of the calculated transition amplitudes in ion-cluster collisions [5–7]. Fragmentation was investigated typically within the framework of statistical theories such as the RRKM Theory of Unimolecular Reactions [8–10], the combination of fast quantum chemical methods with molecular dynamics [11] or the Weisskopf model for cluster fission [12–14].

Despite these efforts, the knowledge of the redistribution of the internal energy in a molecule after collision and its influence on the fragmentation process is still scarce. Recently, Xie et al. studied the effect of the distribution of the vibrational states on nonadiabatic photodissociation of phenol [15]. Nonadiabatic excited state molecular dynamics (NA-ESMD) [16] methodology has proven to be an appropriate tool for the investigation of nonradiative relaxation of excited electronic states. Such investigations focus on the identification of normal modes that participate actively in the redistribution of electronic energy during the inter-

[a] Faculty of Applied Physics and Mathematics, Gdańsk University of Technology, Narutowicza 11/12, 80-233 Gdańsk, Poland. E-mail: marta.labuda@pg.edu.pl
[b] Departamento de Química, Facultad de Ciencias, Módulo 13, Universidad Autónoma de Madrid, 28049 Madrid, Spain.
[c] Theoretical Division, Los Alamos National Laboratory, Los Alamos, New Mexico 87545, United States.
[d] Normandie Univ, ENSICAEN, UNICAEN, CEA, CNRS, CIMAP, 14000 Caen, France.
[e] CNR - Istituto di Struttura della Materia, Area della Ricerca di Roma 1, Monterotondo Scalo, Italy.
[f] Dipartimento di Scienze, Università di Roma Tre, 00146 Roma, Italy.
[g] Elettra-Sincrotrone Trieste, Basovizza, Italy.
[h] Institute for Advanced Research in Chemical Sciences (IAdChem), Universidad Autónoma de Madrid, 28049 Madrid, Spain.
[i] Condensed Matter Physics Center (IFIMAC), Universidad Autónoma de Madrid, 28049 Madrid, Spain.
[j] Instituto Madrileño de Estudios Avanzados en Nanociencias (IMDEA-Nanociencia), 28049 Madrid, Spain.

† Electronic Supplementary Information (ESI) available: Channels distribution as a function of the internal energy calculated with ADMP; Potential energy profiles; Details of M_3C calculations; Fragments database for the M_3C calculations; Explanation of the fitting procedure; Procedure for calculating mass spectral matching score; Energy distributions for other ions; Photoelectron spectrum of furan. See DOI: 10.1039/cXCP00000x/

nal conversion process[17]. However, statistical energy redistribution occurs in a time span of a few vibrations ($<10^{-10}$ s)[18] and due to the coupling between the electronic and vibrational degrees of freedom, the parent ion relaxes via an internal energy dependent molecular fragmentation. Hence, it is possible to study the fragmentation separately from the excitation process. Gas phase collision experiments help to elucidate the very first steps of this complicated chain of events by providing well-defined laboratory conditions. For instance, photoelectron-photoion coincidence (PEPICO) spectroscopy provides state-selected mass spectrometric information, where the fragmentation pattern of specific molecular orbitals (i.e. at fixed internal energies of the cation) can be measured[19]. However, also in this technique the progression of the energy redistribution remains unknown as only the initial internal energy of the ion and the final fragmentation products can be correlated. In particle collision experiments the situation is even more challenging because the determination of the initial internal energy deposited in the collision would require the detection and analysis of the charge state and energy loss of the scattered projectile, measured in coincidence with that of the ejected electron(s)[20]. This complex technique has been applied only in few experiments. For example in ref.[2], the energy loss of the projectile after double electron capture ($Cl^+ \rightarrow Cl^-$) from adenine molecules was measured, or in the case of multi-electron capture collisions of highly charged ions with Na metal clusters[21], where the branching ratios of specific fragments were analyzed to yield information on the internal energies of fragmenting clusters as a function of the projectile charge. The transferred energies were found to decrease strongly with the projectile charge.

The studied molecule - furan (C_4H_4O) - has a planar, five-membered cyclic structure with an oxygen heteroatom. It is a simplified structure of the tetrahydrofuran molecule, often taken as prototype of the DNA deoxyribose, that plays a role in combustion chemistry, polymer science and biologically active substances[22]. Thus, several studies of furan by photoionization and photofragmentation[23–26] including threshold photoelectron-photoion coincidence (TPEPICO)[27,28] and electron impact ionization[29] experiments, have been reported in the literature.

Here, we report a joint theoretical and experimental study which aims to establish a universal framework for the investigation of molecular fragmentation after an ionizing event. The essence of our strategy is to combine *ab initio* quantum chemistry methods with a recently developed statistical technique[30,31] to describe the redistribution of the internal energy transferred to a molecular target by photoionization or particle collision and its effect on the fragmentation yields. For this purpose, we use the Microcanonical Metropolis Monte Carlo method, in its recent implementation in the M_3C code[31,32] to evaluate the assumption of a fast and efficient coupling between electronic and vibrational degrees of freedom. Previously, we focused our attention on a more straightforward unimolecular decomposition of neutral furan molecules[33]. PEPICO is used to validate the theoretical approach which could thus be applied to determine the energy transfer and redistribution in ion-collision and electron impact experiments. The direct comparison with the PEPICO experiments provides a systematic means of evaluating the accuracy and applicability of this new methodology. Additionally, it reveals several specific, previously unknown, multi-step fragmentation pathways of excited singly-ionized furan; thus providing further insights into the fragmentation mechanisms.

2 Methods

2.1 Computational methods

The theoretical strategy presented here consists of three, complementary approaches, focusing on the dynamical, energetic and entropic aspects of the studied processes. Firstly, *ab initio* molecular dynamics simulations (with a maximum propagation time of 500 fs and time step of 0.1 fs) are carried out with the Atom Centered Density Matrix Propagation method[34–36] and the B3LYP[37,38] functional combined with the 6-31G(d,p) basis set. The energies between 5 eV and 30 eV in steps of 1 eV are deposited into the furan cation and randomly distributed over all nuclear degrees of freedom. Vertical excitation is modelled by taking equilibrium geometry of the neutral furan molecule after removal of one electron as an initial step in the molecular dynamics simulations. For each energy 150 trajectories have been calculated, giving together 3900 trajectories. Bond distances and charge distributions at the last dynamical step (500 fs) of every trajectory are used to detect reactive mechanisms. Bonds are assumed to be broken when the distance between atoms exceeded R = 2.5 Å. Even though the molecule is still expected to fragment after 500 fs, such simulation time proved to give enough insight into the mechanism of fragmentation and possible products. Distributions of channels corresponding to different processes are given in figure S1 of the ESI†. Secondly, based on the distribution of channels and mechanisms observed in the dynamical simulations, critical points on the potential energy surface are optimized at the B3LYP/6-311++G(d,p) level of theory. Both quantum chemical methods are implemented in the Gaussian09 software package[39]. To localize critical points (local minima and transition states), the Berny algorithm using GEDIIS[40] is used in redundant internal coordinates as it is implemented in Gaussian09 (default option). No special options were required. The initial guesses of the geometries are created by a random sampling of the reactive molecular-dynamics trajectories described above. Some transition state optimizations required manual modifications in the initial geometry to reach convergence. Finally, the M_3C statistical approach[30,31] in a constrained manner[41] introduces entropy maximization as a procedure for obtaining fragmentation branching ratios. The M_3C method considers statistical space averages instead of time averages according to the ergodic theorem and considers only the total energy of the produced fragments, neglecting the possible presence of energy barriers on the fragmentation path. However, especially at lower internal energy values, the omission of energy barriers may cause erroneous results. Therefore, it is necessary to explore the potential energy surface in order to locate significantly high energy barriers associated with relevant fragmentation pathways. The molecular dynamics simulations and the exhaustive exploration of the potential energy surface ensure the location of such barriers.

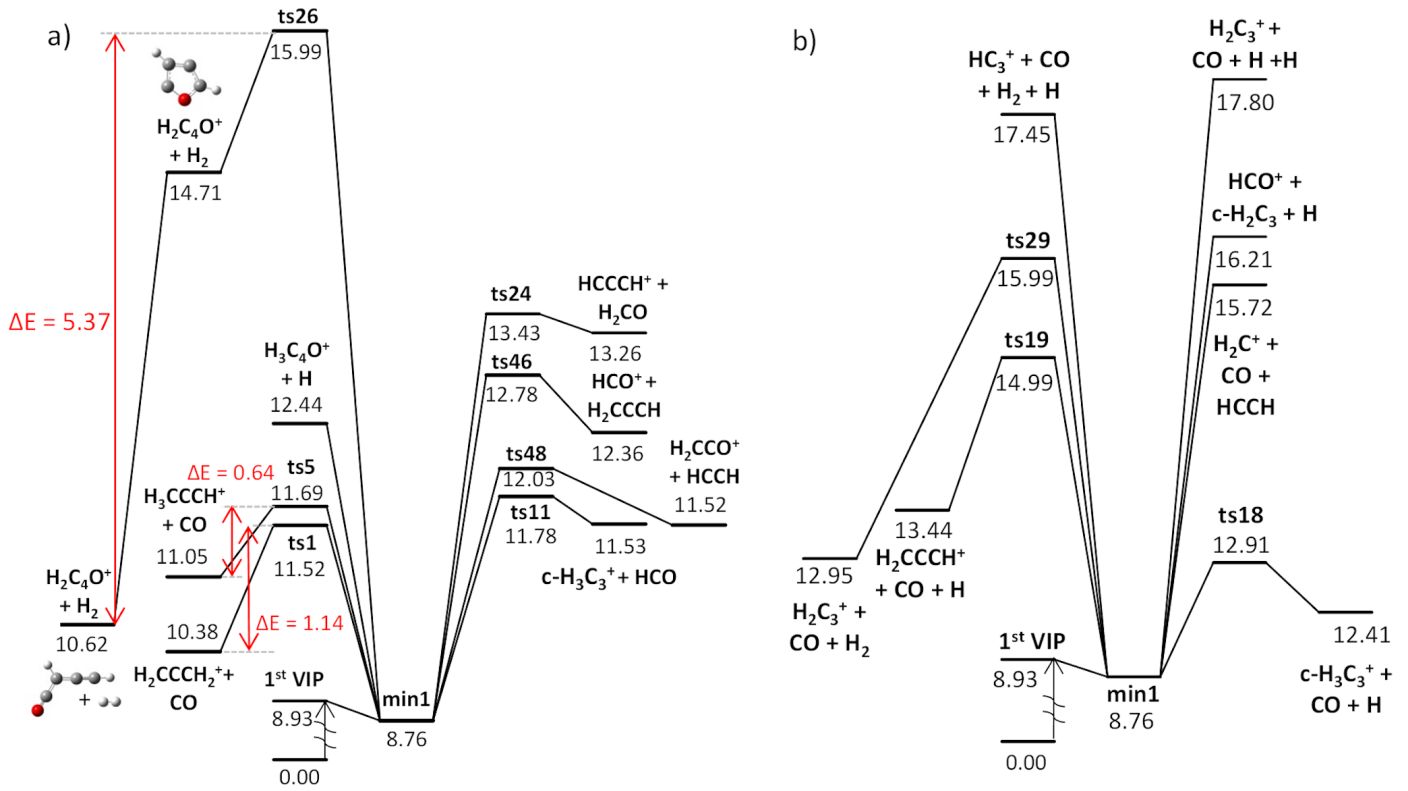

Fig. 1 Simplified potential energy profiles of the two-body (a) and three-/four-body (b) fragmentation channels of the furan cation. Relative energies with respect to the lowest energy state of the neutral furan are given in eV. Red arrows indicate the increase in the energy of the corresponding fragmentation channels introduced in the M_3C input data.

2.2 Experimental methods

The PEPICO experiments have been performed at the GasPhase Photoemission beamline of the Elettra synchrotron radiation source. A photon beam of 60 eV interacts with an effusive beam of furan molecules and the photoelectron and photoion are detected in time-coincidence, by a hemispherical analyzer and a time-of-flight spectrometer, respectively, mounted back-to-back at the pseudo magic angle with respect to the fully linearly polarized radiation[42]. At selected binding energy (BE) values identified by the kinetic energy of the detected photoelectron, the energy selected mass spectrum is measured. The relative intensity of the parent and fragment ions in each PEPICO spectrum reported versus BE produces the breakdown curves, i.e. the evolution of the branching ratio of specific fragments versus ions' BE. In the analysis, only processes leading to single ionization have been selected. In the following, the term "internal energy" will be used to indicate the BE-IE difference, where IE is the vertical ionization energy. Thus, this difference is the excitation energy deposited in the molecular ion during the ionizing process.

The ion-induced fragmentation experiments have been performed at the low energy ion beam facility ARIBE of GANIL in Caen (France)[43] with a crossed-beam device described in details elsewhere[44], thus only a brief description is given here. Low–energy ions are produced in an electron cyclotron resonance ion source. They are extracted, mass-selected, pulsed (pulse length 0.5 μs for multiply charged ions and 3 μs for the singly charged one) and transported to the experimental area, where they cross a molecular effusive beam. After collimation, the different beam intensities are $\sim$ 60 pA for 3 keV Ar^+ ions and $\sim$ 20 pA for multiply charged ion species. The molecular beam was produced by evaporation of a commercially purchased furan sample (99% purity, Sigma Aldrich) was kept at room temperature in a glass tube drown in a water tank to ensure stable temperature during experiments. This simple set-up configuration allows to obtain a sufficient vapor density without any heating of the liquid sample. After the interaction, cationic products are orthogonally extracted into a modified Wiley-McLaren linear time-of-flight TOF mass spectrometer[45]. After passing the 1m long drift region the mass-over-charge analyzed cations are strongly post-accelerated before impacting a conversion plate. Emitted secondary electrons are guided by a weak magnetic field towards a channel plate detector. In this way, high detection efficiency is obtained independently of the ion mass. The arrival times are digitized with 1 ns resolution in an event-by-event mode (FAST ComTec P7888). Using a low intensity ion beam allows to obtain conditions where the number of charged particles produced within one ion pulse is negligibly small, thus several fragments detected per ion pulse are due to a single collision event. Therefore, each event is characterized by the number of detected fragments and their TOFs in such a way that the correlation between them can be studied[46].

3 Results

The potential energy surface exploration results are summarized in Figure 1 with the fragmentation pathways of two-, three- and

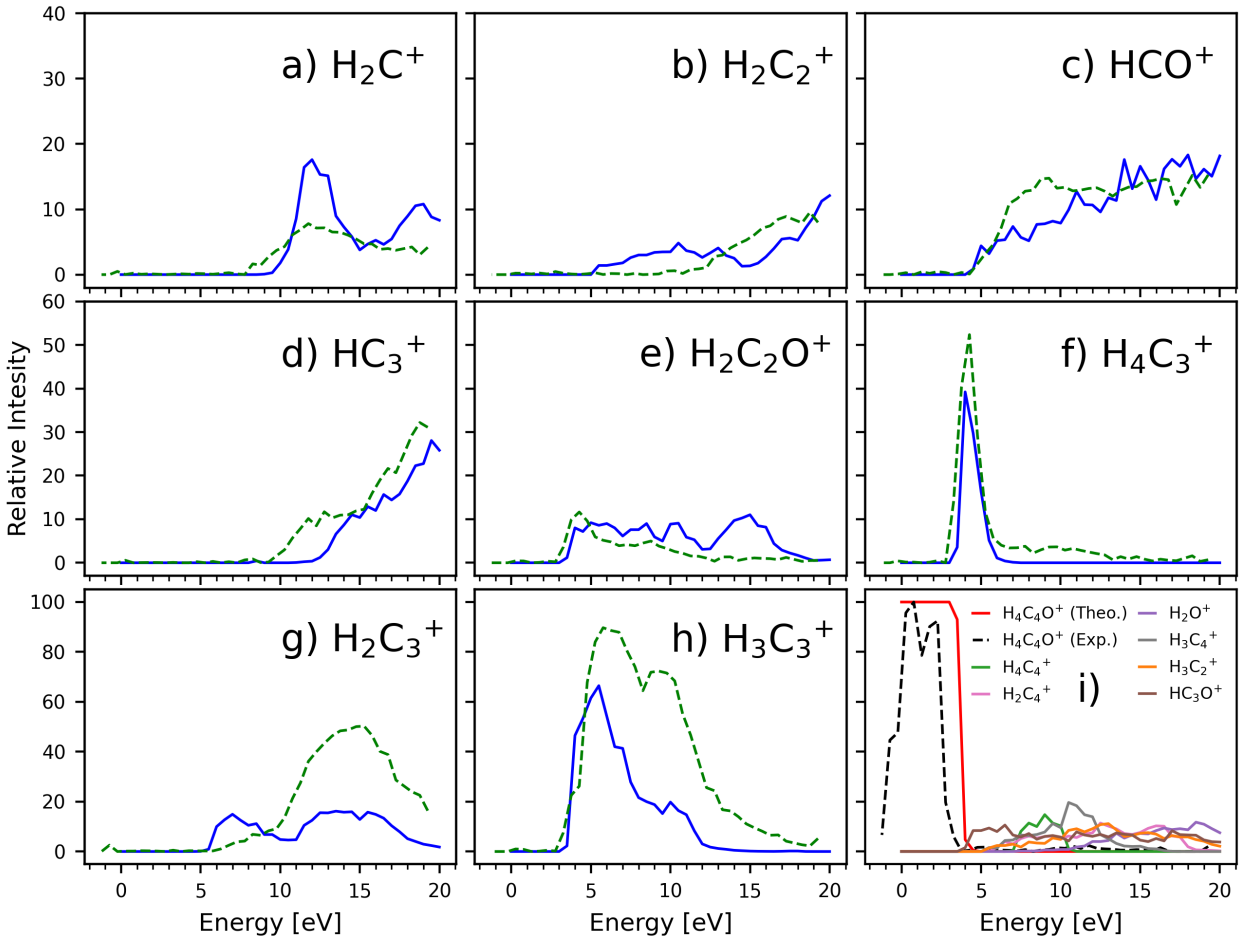

Fig. 2 Comparison of the breakdown curves calculated with the M_3C method (solid) and measured in the PEPICO experiment (dashed). Lowest right panel collects the breakdown curves of fragments predicted by M_3C with probability higher than 10%, but not observed in the PEPICO experiment as well as the measured and calculated intensities of parent cation. The average error in the M_3C calculated breakdown curves (standard deviation) was converged up to 7%.

four-body channels. Among the two-body processes, the most important channels involving skeleton fragmentation, ordered according to increasing values of the calculated energy barriers (see Figure 1a) are: $H_4C_3^+$ + CO, $H_3C_3^+$ + HCO, $H_2C_2O^+$ + H_2C_2 and HCO^+ + H_3C_3. Three- and four-body decomposition channels mostly consist of hydrogen losses and subsequent fragmentation. For the three-body fragmentation, the lowest energy pathway was calculated for channel $H_3C_3^+$ + CO + H, while the four-body fragmentation can produce fragments $H_2C_3^+$ and HC_3^+ (see Figure 1b). The full potential energy profiles with structures of transition states and products are presented in the section SI.2 of ESI†.

A direct comparison between the PEPICO measured breakdown curves and the calculated M_3C fragmentation probabilities of the most significant ions is shown in Figure 2. Based on the initial comparison between the height of the barriers in the potential energy surface and the calculated M_3C breakdown curves, we found it mandatory to artificially introduce energy barriers leading to the production of fragments $H_4C_3^+$ and $H_2C_4O^+$, i.e. for the lowest energy channels, by increasing the energy of specific fragments in the database (see Figure 1a and ESI† for further details). In general, the M_3C breakdown curves are consistent with the experimental ones, except for the two maxima predicted for the H_2C^+ and $H_2C_3^+$ fragments and the different intensities for the fragments $H_2C_3^+$ and $H_3C_3^+$. The latter can be attributed to a number of species obtained in the M_3C calculations, but not observed in PEPICO (panel i) of Figure 2). Despite their relatively low intensity, they can alter the overall budget of the "total ion yield" and decrease the branching ratio of $H_2C_3^+$, $H_3C_3^+$ and other species.

Detailed investigation of the production mechanisms of the significant fragments and the accuracy of their calculated breakdown curves with respect to the experimental ones is crucial for proving the adequacy of the proposed method. The lowest energy barrier for fragmentation of the furan ring is equal to 11.52 eV with respect to the neutral furan (i.e. 2.59 eV over IE) and produces the $H_4C_3^+$ fragment in the allene form and CO. This pathway proceeds through several transition states that involve molecular rearrangements and ring opening (see Figures 1 and S3 in ESI†). The calculated value for this barrier is fully consistent with the appearance energy (AE) reported in the literature[28]

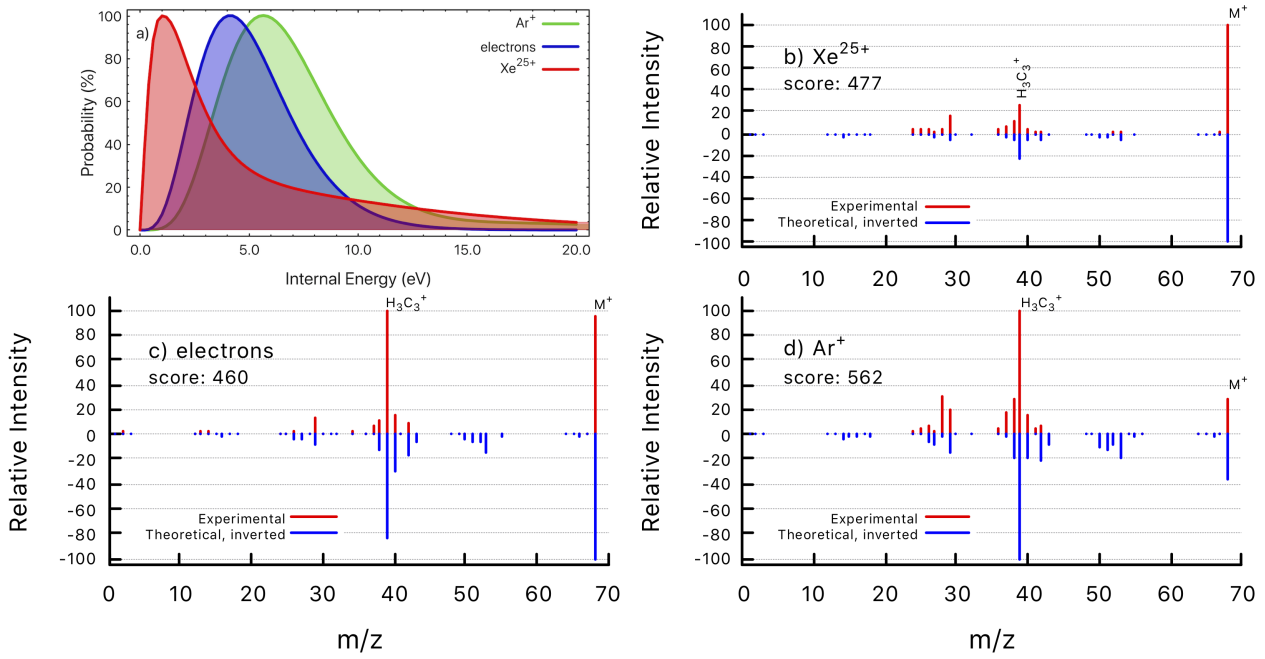

Fig. 3 (a) Determined distributions of internal energy in the ion collision and electron impact experiments. (b)-(d) Experimental mass spectra (red) detected after the interaction of Xe^{25+} (b), electrons (c) and Ar^+ (d) with furan molecule. Inverted peaks (blue) are theoretical mass spectra obtained by convolution of M_3C breakdown curves with the corresponding internal energy function from panel (a). Mass spectral matching scores are indicated on respective mass spectra.

and the take-off of the corresponding PEPICO breakdown curve in Figure 2. Accordingly, the branching ratio calculated with M_3C is also in very good agreement with the measured one.

The fragmentation channel $H_3C_3^+$ + HCO does not require hydrogen transfer and relies only on the cleavage of the C-O and C-C bonds. As a result, a cyclic isomer of $H_3C_3^+$ is expected to be the most abundant product of furan cation fragmentation. In this case the predicted energy barrier (transition state ts11 at 11.78 eV) is about 0.3 eV below the experimental AE[28] (see Figures 1 and S4). Both experimental and theoretical results in Figure 2 indicate that $H_3C_3^+$ is the most abundant species in the internal energy range 5 – 11 eV, even though the calculated branching ratio underestimates the measured one by about 30%. The detailed analysis of the M_3C simulations for this channel indicates that the second peak in the PEPICO breakdown curve around 11 eV results from H loss mechanisms, in which $H_3C_3^+$ is produced in a linear conformer.

Channel $H_2C_2O^+$ + H_2C_2 (details in Figure S7) has a calculated energy barrier of 12.03 eV. The proposed mechanism consists in a two-step process: hydrogen migration followed by the ring opening. The calculated branching ratio is in good agreement with the measured PEPICO breakdown curve in the internal energy range 4-10 eV, predicting a non-negligible intensity above 10 eV, not observed in the experimental data. Finally, in the case of HCO^+ + H_3C_3 with a calculated energy barrier of 12.78 eV (see Figure S7) a very good agreement between the calculated and measured breakdown curves is obtained as shown in Figure 2.

The mass spectra produced by single ionization of furan by two different ions (3 keV Ar^+ and 565 keV Xe^{25+}) and 100 eV electrons[29] are presented in Figure 3b-d. The fragmentation induced by other projectiles as O^{3+}, O^{6+} and Ar^{11+} has been also studied and the results are presented in the ESI†. The fragmentation patterns depend on the projectile and its charge state. As the charge increases less fragmentation is observed and the parent cation dominates the spectrum. Moreover, as in the case of the fragmentation of polycyclic hydrocarbon species[47], the fragments appear in groups due to the loss of a single or several heavy particles accompanied by multiple hydrogen losses, see e.g. the clustered features at m/z 24-32 and 36-44. Besides the parent ion, the most prominent peak corresponds to the $H_3C_3^+$ fragment, as also observed in the PEPICO experiments.

4 Discussion

The good agreement between calculated and measured branching ratios suggests that the amount of the energy transferred to the fragmenting system and, thus, the resulting internal energy distribution function is the main parameter which determines the fragmentation pattern. Thus, it should be independent of the applied excitation, ionization method. This is in line with the assumption that the excess energy can be distributed randomly among all internal degrees of freedom. Therefore, from the calculated breakdown curves we can determine backwards the internal energy distribution function for the ion-molecule collision and electron impact experiments as that one which generates the best fit to each measured mass spectrum (see details in section SI.5 in ESI†).

The level of similarity between experimental and theoretically reproduced mass spectra can be quantified by a mass spectral matching score[48]. The composite score, previously applied among others to assess computed electron ionization mass spec-

tra[49], can take the values between 0 (no similarity) and 1000 (identical spectra). This score puts emphasis on more informative higher mass peaks and accounts for similarities in the neighboring peaks topology. In the present work, the scores range from 451 to 562. Composite score values around 500 have been previously considered as satisfactory[50]. Although the most important peaks are well reproduced (parent ion and $H_3C_3^+$) decreased matching score can be attributed to a too high number of peaks predicted by theory, which is included in the denominator of the calculated score (see ESI†section SI.6 for more details). Interestingly, theoretical mass spectra show additional, small peaks at m/z 50, 51, 52, and 53 compared to the experimental ones. These m/z values correspond to the $H_2C_4^+$, $H_3C_4^+$, $H_4C_4^+$, and HC_3O^+ fragments, respectively. The fact that these fragments are observed in theory but not in the experiment is again due to the lack of inclusion of barriers in the reactions preceding those fragments' production during the statistical simulation. The production of these fragments would progress through many H transfers and unlikely O or OH loss (see ESI†). Certainly, the approximation we have done by assuming that these reactions will happen without barriers and in a single step is imprecise. Nevertheless, such an approach is good enough to provide sufficient agreement with the experiment in the explored energy ranges.

The obtained internal energy distributions are shown in Figure 3a and Figure S9. A clear shift of the maximum towards larger energy values in the M_3C calculated internal energy distribution can be observed as the ion charge decreases from Xe^{25+} to Ar^+. This result is consistent with the fact that single electron capture occurs at much larger ion-molecule distances for higher projectile charges[20], hence leading to a much lower energy transfer[21,51]. Figure 3a shows that the internal energy distributions for Ar^+ and electrons present maxima at 6 and 4 eV, respectively. In these cases, ionization occurs in close or penetrating collisions by either electron capture or direct ionization. However, in the case of Xe^{25+} the distribution peaks around 1 eV and then extends up to 20 eV, representing collisions at large and small impact parameters, respectively, with a predominance for the former. Energy distributions for other ions are given in Figure S9. This qualitative agreement proves the adequacy and generality of the proposed methodology.

We can also use the results of the M_3C simulations to obtain information on the redistribution of the excitation energy among its different components: translational, vibrational and rotational energy and intermolecular energy. The latter is defined as the sum of the electronic energy of the fragments (relative to the parent ion) in a given fragmentation channel[31]. The different components are shown in Figure 4. In the region of lower internal energies, the vibrational energy is the main component of the total energy, as the molecule remains intact and therefore it is crucial to correctly predict and understand the fragmentation patterns. The contribution of this component decreases until fragmentation becomes the dominant process and remains at the level of 30-40 %. Above 4 eV, the most significant component is the intermolecular energy associated with the bond breaking.

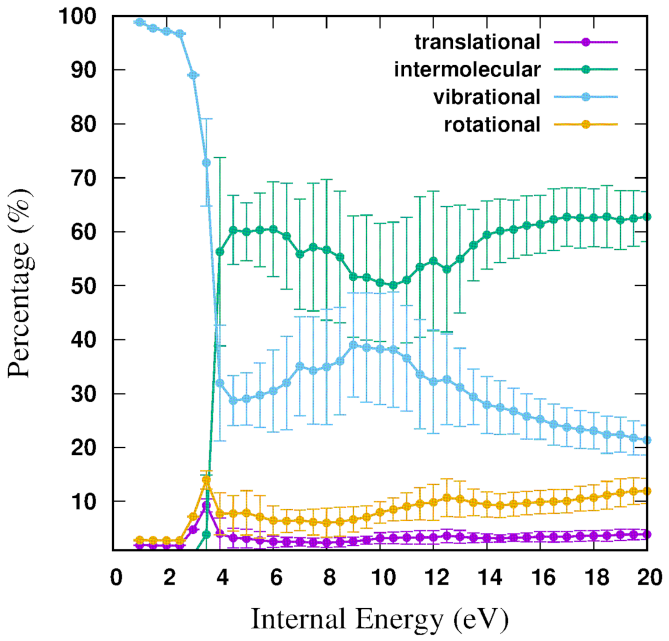

Fig. 4 M_3C energy components as a function of the total energy. Error bars correspond to standard deviation of mean probabilities over all numerical experiments.

5 Conclusions

In summary, this combined experimental and theoretical study has allowed to i) give a detailed description of the fragmentation pathways, ii) deliver the first report of theoretical breakdown curves for the furan cation based on the combination of high level quantum chemical calculations and a statistical Monte Carlo method, iii) determine the internal energy distributions after charged particle collisions. The agreement of the PEPICO measurements and M_3C calculations confirms the efficiency of a statistical exchange of internal energy between various degrees of freedom. When compared to the standard statistical RRKM theory, typically employed in the studies of the fragmentation processes, the M_3C method proves to be more suitable for studying systems in which energy barriers do not play a key role or the reverse barriers are minimal. In particular for larger systems, in which hundreds of possible fragmentation channels follow barrierless transitions, the M_3C methodology is preferable to the RRKM theory. For example, for furan cation fragmentation, it is necessary to consider more than two thousand reactions. From the RRKM perspective, it would be necessary to use the variational RRKM technique (see e.g.[52]), which requires special dedication to every reaction happening in the system. In particular, late transition states are quite difficult to describe due to the basis of the approach involving a separation of the vibrational modes into "conserved" and "transitional" modes that become free rotations in the transition state. This complexity makes the RRKM methodology unfit to be automated on large systems like furan cation due to the large number of barrierless reactions to consider. The inclusion of two energy barriers in the reaction network in the present work already provided good agreement with the experi-

mental breakdown curves. The results also support the assumption, intrinsic in the M_3C method, that the fragmentation is independent of the excitation process, i.e. the applied excitation and ionization method. This underlines the scientific potential of the method. The proposed approach, on the one hand, might guide new efforts to unravel the molecular fragmentation of more complex systems like large biomolecules and, on the other hand, find useful applications in the modelling of radiation damage. It is especially important, for example, in ion-beam cancer therapy and energetic processing of nanosystems.

Conflicts of interest

There are no conflicts to declare.

Acknowledgements

This article is based upon work from the COST Action CA18212 - Molecular Dynamics in the GAS phase (MD-GAS), supported by COST (European Cooperation in Science and Technology). We thank the Erasmus Plus Programme (M.Ł.) and Gdańsk University of Technology (M.Ł. and E.E.) for financial support. M.Ł. thanks the Ambassade de France en Pologne for the French Government Scholarship for Researchers to visit the GANIL facility. We acknowledge the allocation of computer time at Academic Computer Centre in Gdańsk (CI TASK), Wrocław Centre for Networking and Supercomputing (WCSS) and Centro de Computación Científica at the Universidad Autónoma de Madrid (CCC-UAM). The research was conducted in the framework of the International Associated Laboratory (LIA) "Fragmentation DYNAmics of complex MOlecular systems" (DYNAMO) and of the International Program for Scientific Collaboration (PICS) "BIomolecular Ions: from Fundamental to Applied scienCE" (BIFACE), both funded by the Centre National de la Recherche Scientifique (CNRS). This work was partially supported by the project CTQ2016-76061-P of the Spanish Ministerio de Economía y Competitividad (MINECO). Financial support from the MINECO through the "María de Maeztu" Program for Units of Excellence in R&D (MDM-2014-0377) is also acknowledged.

Notes and references

1 L. Chen, S. Martin, J. Bernard and R. Brédy, *Physical Review Letters*, 2007, **98**, 6–9.

2 R. Brédy, J. Bernard, L. Chen, G. Montagne, B. Li and S. Martin, *The Journal of Chemical Physics*, 2009, **130**, 114305.

3 S. Maclot, R. Delaunay, D. Piekarski, A. Domaracka, B. Huber, L. Adoui, F. Martín, M. Alcamí, L. Avaldi, P. Bolognesi and P. Rousseau, *Physical Review Letters*, 2016, **073201**, 1–6.

4 T. Chen, M. Gatchell, M. H. Stockett, J. D. Alexander, Y. Zhang, P. Rousseau, A. Domaracka, S. Maclot, R. Delaunay, L. Adoui, B. A. Huber, T. Schlathölter, H. T. Schmidt, H. Cederquist and H. Zettergren, *Journal of Chemical Physics*, 2014, **140**, year.

5 P.-A. Hervieux, B. Zarour, J. Hanssen, M. Politis and F. Martín, *Journal of Physics B*, 2001, 3331–3355.

6 P.-A. Hervieux, L. F. Ruiz, S. Díaz-Tendero, M. Alcamí, B. Zarour, M. F. Politis, J. Hanssen and F. Martín, *Physica Scripta*, 2004, **110**, 308.

7 A. Rentenier, L. F. Ruiz, S. Díaz-Tendero, B. Zarour, P. Moretto-Capelle, D. Bordenave-Montesquieu, A. Bordenave-Montesquieu, P. A. Hervieux, M. Alcamí, M. F. Politis, J. Hanssen and F. Martín, *Physical Review Letters*, 2008, **100**, 183401.

8 O. K. Rice and H. C. Ramsperger, *Journal of the American Chemical Society*, 1927, **49**, 1617–1629.

9 L. S. Kassel, *The Journal of Physical Chemistry*, 1928, **32**, 1065–1079.

10 R. A. Marcus, *The Journal of Chemical Physics*, 1952, **20**, 359–364.

11 S. Grimme, *Angewandte Chemie International Edition*, 2013, **52**, 6306–6312.

12 V. Weisskopf, *Physical Review*, 1937, **52**, 295–303.

13 G. Martinet, S. Díaz-Tendero, M. Chabot, K. Wohrer, S. D. Negra, F. Mezdari, H. Hamrita, P. Désesquelles, A. L. Padellec, D. Gardés, L. Lavergne, G. Lalu, X. Grave, J. F. Clavelin, P. A. Hervieux, M. Alcamí and F. Martín, *Physical Review Letters*, 2004, **93**, 063401.

14 H. da Silva, J. Oller, M. Gatchell, M. H. Stockett, P.-A. Hervieux, L. Adoui, M. Alcamí, B. A. Huber, F. Martín, H. Cederquist, H. Zettergren, P. Rousseau and S. Díaz-Tendero, *Physical Review A*, 2014, **90**, 032701.

15 C. Xie, B. Zhao, C. L. Malbon, D. R. Yarkony, D. Xie and H. Guo, *The Journal of Physical Chemistry Letters*, 2020, **11**, 191–198.

16 T. Nelson, S. Fernandez-Alberti, V. Chernyak, A. E. Roitberg and S. Tretiak, *The Journal of Physical Chemistry B*, 2011, **115**, 5402–5414.

17 P. M. Shenai, S. Fernandez-Alberti, W. P. Bricker, S. Tretiak and Y. Zhao, *The Journal of Physical Chemistry B*, 2016, **120**, 49–58.

18 E. de Hoffmann and V. Stroobant, *Mass Spectrometry: Principles and Applications*, Wiley, 3rd edn, 2007.

19 P. Bolognesi and L. Avaldi, *Nanoscale Insights into Ion-Beam Cancer Therapy*, Springer International Publishing, 2017, pp. 209–235.

20 P. Rousseau and B. A. Huber, *Nanoscale Insights into Ion-Beam Cancer Therapy*, Springer International Publishing, 2017, pp. 121–157.

21 F. Chandezon, H. Lebius, S. Tomita, C. Guet, A. Pesnelle and B. A. Huber, *Physica Scripta*, 2001, **T92**, 168–170.

22 O. Meth-Cohn, C. Rees and A. Katritzky, *Comprehensive Heterocyclic Chemistry: the Structure, Reactions, Synthesis and Uses of Heterocyclic Compounds vol. 1*, Oxford: Pergamon, 1984.

23 K. Kimura, *Handbook of HeI Photoelectron Spectra of Fundamental Organic Molecules*, Japan Scientific Societies Press, 1981.

24 G. Bieri, L. Åsbrink and W. von Niessen, *Journal of Electron Spectroscopy and Related Phenomena*, 1982, **27**, 129–178.

25 A. Bawagan, B. Olsson, K. Tan, J. Chen and B. Yang, *Chemical Physics*, 1992, **164**, 283 – 304.

26 E. Rennie, C. Johnson, J. Parker, D. Holland, D. Shaw, M. Mac-

Donald, M. Hayes and L. Shpinkova, *Chemical Physics*, 1998, **236**, 365–385.

27 G. D. Willett and T. Baer, 1980, **102**, 6769–6773.

28 E. E. Rennie, L. Cooper, C. A. Johnson, J. E. Parker, R. A. Mackie, L. G. Shpinkova, D. M. Holland, D. A. Shaw and M. A. Hayes, *Chemical Physics*, 2001, **263**, 149–165.

29 M. Dampc, I. Linert and M. Zubek, *Journal of Physics B: Atomic, Molecular and Optical Physics*, 2015, **48**, 165202.

30 S. Díaz-Tendero, P.-A. Hervieux, M. Alcamí and F. Martín, *Physical Review A*, 2005, **71**, 033202.

31 N. F. Aguirre, S. Díaz-Tendero, P.-A. Hervieux, M. Alcamí and F. Martín, *Journal of Chemical Theory and Computation*, 2017, **13**, 992–1009.

32 N. F. Aguirre, S. Díaz-Tendero, P.-A. Hervieux, M. Alcamí and F. Martín, *M3C (Microcanonical Metropolis Monte-Carlo)*, 2020, `https://github.com/nfaguirrec/M3C`.

33 E. Erdmann, M. Łabuda, N. F. Aguirre, S. Díaz-Tendero and M. Alcamí, *The Journal of Physical Chemistry A*, 2018, **122**, 4153–4166.

34 H. B. Schlegel, J. M. Millam, S. S. Iyengar, G. A. Voth, A. D. Daniels, G. E. Scuseria and M. J. Frisch, *Journal of Chemical Physics*, 2001, **114**, 9758–9763.

35 S. S. Iyengar, H. B. Schlegel, J. M. Millam, G. A. Voth, G. E. Scuseria and M. J. Frisch, *Journal of Chemical Physics*, 2001, **115**, 10291–10302.

36 H. B. Schlegel, S. S. Iyengar, X. Li, J. M. Millam, G. A. Voth, G. E. Scuseria and M. J. Frisch, *Journal of Chemical Physics*, 2002, **117**, 8694–8704.

37 A. D. Becke, *The Journal of Chemical Physics*, 1993, **98**, 5648–5652.

38 C. Lee, W. Yang and R. G. Parr, *Physical Review B*, 1988, **37**, 785–789.

39 M. J. Frisch, G. W. Trucks, H. B. Schlegel, G. E. Scuseria, M. A. Robb, J. R. Cheeseman, G. Scalmani, V. Barone, G. A. Petersson, H. Nakatsuji, X. Li, M. Caricato, A. V. Marenich, J. Bloino, B. G. Janesko, R. Gomperts, B. Mennucci, H. P. Hratchian, J. V. Ortiz, A. F. Izmaylov, J. L. Sonnenberg, D. Williams-Young, F. Ding, F. Lipparini, F. Egidi, J. Goings, B. Peng, A. Petrone, T. Henderson, D. Ranasinghe, V. G. Zakrzewski, J. Gao, N. Rega, G. Zheng, W. Liang, M. Hada, M. Ehara, K. Toyota, R. Fukuda, J. Hasegawa, M. Ishida, T. Nakajima, Y. Honda, O. Kitao, H. Nakai, T. Vreven, K. Throssell, J. A. Montgomery, Jr., J. E. Peralta, F. Ogliaro, M. J. Bearpark, J. J. Heyd, E. N. Brothers, K. N. Kudin, V. N. Staroverov, T. A. Keith, R. Kobayashi, J. Normand, K. Raghavachari, A. P. Rendell, J. C. Burant, S. S. Iyengar, J. Tomasi, M. Cossi, J. M. Millam, M. Klene, C. Adamo, R. Cammi, J. W. Ochterski, R. L. Martin, K. Morokuma, O. Farkas, J. B. Foresman and D. J. Fox, *Gaussian 09 Revision E.01*, 2016, Gaussian Inc. Wallingford CT.

40 X. Li and M. J. Frisch, *Journal of Chemical Theory and Computation*, 2006, **2**, 835–839.

41 N. F. Aguirre, S. Díaz-Tendero, T. IdBarkach, M. Chabot, K. Béroff, M. Alcamí and F. Martín, *The Journal of Chemical Physics*, 2019, **150**, 144301.

42 P. Bolognesi, J. A. Kettunen, A. Cartoni, R. Richter, S. Tosic, S. Maclot, P. Rousseau, R. Delaunay and L. Avaldi, *Phys. Chem. Chem. Phys.*, 2015, **17**, 24063–24069.

43 V. Bernigaud, O. Kamalou, A. Lawicki, M. Capron, R. Maisonny, B. Manil, L. Maunoury, J. Rangama, P. Rousseau, J. Y. Chesnel, L. Adoui and B. A. Huber, *Publications of the Astronomical Observatory of Belgrade*, 2008, **84**, 83–86.

44 T. Bergen, X. Biquard, A. Brenac, F. Chandezon, B. A. Huber, D. Jalabert, H. Lebius, M. Maurel, E. Monnand, J. Opitz, A. Pesnelle, B. Pras, C. Ristori and J. C. Rocco, *Review of Scientific Instruments*, 1999, **70**, 3244–3253.

45 F. Chandezon, B. Huber and C. Ristori, *Review of Scientific Instruments*, 1994, **65**, 3344–3353.

46 M. Capron, S. Díaz-Tendero, S. Maclot, A. Domaracka, E. Lattouf, A. Ławicki, R. Maisonny, J.-Y. Chesnel, A. Méry, J.-C. Poully, J. Rangama, L. Adoui, F. Martín, M. Alcamí, P. Rousseau and B. A. Huber, *Chemistry – A European Journal*, 2012, **18**, 9321–9332.

47 P. Rousseau, A. Ławicki, A. Holm, M. Capron, R. Maisonny, S. Maclot, E. Lattouf, H. Johansson, F. Seitz, A. Méry, J. Rangama, H. Zettergren, S. Rosén, H. Schmidt, J.-Y. Chesnel, A. Domaracka, B. Manil, L. Adoui, H. Cederquist and B. Huber, *Nuclear Instruments and Methods in Physics Research Section B: Beam Interactions with Materials and Atoms*, 2012, **279**, 140 – 143.

48 S. E. Stein and D. R. Scott, *Journal of the American Society for Mass Spectrometry*, 1994, **5**, 859–866.

49 C. A. Bauer and S. Grimme, *The Journal of Physical Chemistry A*, 2014, **118**, 11479–11484.

50 C. A. Bauer and S. Grimme, *The Journal of Physical Chemistry A*, 2016, **120**, 3755–3766.

51 S. Maclot, D. G. Piekarski, R. Delaunay, A. Domaracka, A. Méry, V. Vizcaino, J.-Y. Chesnel, F. Martín, M. Alcamí, B. A. Huber, L. Adoui, P. Rousseau and S. Díaz-Tendero, *The European Physical Journal D*, 2014, **68**, 149.

52 J. L. Bao and D. G. Truhlar, *Chem. Soc. Rev.*, 2017, **46**, 7548–7596.